



## Heavy fermion related behaviors and the effects from nonmagnetic atom vacancies in the $5f$ -electron based antiferromagnet $UAs_2$

Xingyu Ji , Qin Liu ,\* Wei Feng, Yun Zhang, Qiuyun Chen, Yi Liu, Qunqing Hao, Jian Wu, Ziwei Xue, Xiegang Zhu, Qiang Zhang, Xuebing Luo, Shiyong Tan,<sup>†</sup> and Xinchun Lai<sup>‡</sup>

*Science and Technology on Surface Physics and Chemistry Laboratory, Mianyang 621908, China*



(Received 15 November 2023; accepted 24 January 2024; published 26 February 2024)

Recent studies on the electronic structures of the  $5f$ -electron based antiferromagnetic compounds, i.e., uranium dipnictides, have aroused widespread interest in the complex interplay among different channels of interactions, such as Kondo entanglement and antiferromagnetic ordering. Here, we use scanning tunneling microscopy/spectroscopy to explore the complex low-energy excitations in the  $5f$ -electron based antiferromagnet  $UAs_2$ . The crystal-field excitations are revealed as peaks above the Fermi level in the  $dI/dV$  spectra. Temperature-dependent spectroscopic measurements find that Kondo resonance and antiferromagnetic order are manifested as two peaks below the Fermi level, demonstrating that Kondo coherence can be undisturbedly established in the antiferromagnetic phase. The crystal-field excitations, Kondo resonance, and antiferromagnetic state are all locally altered by the presence of As-atom vacancies at the atomic scale and these phenomena prove that the nonmagnetic atom vacancy has a strong influence on low-energy excitations in heavy fermion compounds.

DOI: [10.1103/PhysRevB.109.075158](https://doi.org/10.1103/PhysRevB.109.075158)

### I. INTRODUCTION

In heavy fermion (HF) materials [1,2], the interaction between the local magnetic moments mediated by spin-polarized conduction electrons forms the Ruderman-Kittel-Kasuya-Yosida (RKKY) interaction [3], which promotes the establishment of magnetic order with decreasing temperature. Meanwhile, at low temperatures, the coupling between local magnetic moments and itinerant conduction electrons via their hybridization leads to the formation of Kondo resonance (KR) near the Fermi level ( $E_F$ ) [4]. In conventional HF theory, these two interactions, i.e., magnetic ordering and the Kondo effect, are thought to compete with each other to determine the ground state. For instance, in the  $4f$  system  $YbRh_2Si_2$ , when it approaches the quantum critical point, antiferromagnetic-ordered (AFM) phase is formed accompanied by the collapse of the Kondo effect [5,6]. Surprisingly, in recent years, KR and AFM are found to coexist with each other in some compounds, such as  $CeSb$  and  $USb_2$  [7–10]. Although the Kondo effect has been extensively studied in various HF compounds [1,11–14], the direct experimental observations of Kondo behavior inside a magnetically ordered phase are still scarce, especially for the  $5f$ -electron based systems [7,8,14,15], and how the Kondo resonance interacts with the magnetic order is still under hot debate. Obviously, more corresponding explorations are highly desired and can deepen our recognition of the intricate relations between the Kondo and AFM states.

Recently, the uranium dipnictides  $UX_2$  ( $X = P, As, Sb, Bi$ ) have attracted considerable attention [7–9,14–16], since  $UX_2$  compounds are ideal systems to explore the interplay between KR and AFM in the magnetic ordered background due to their rather high Néel temperatures ( $T_N$ ) [7–9,14–16]. Angle-resolved photoemission spectroscopy (ARPES) detected different kinds of flat bands respectively related with the AFM state and Kondo entanglement separated in the momentum space in  $USb_2$  and  $UAs_2$  [7,15]. However, different research groups have not reached consensus in the scanning tunneling microscopy/spectroscopy (STM/STS) studies of  $USb_2$  [8,9]. Giannakis *et al.* found a novel first-order-like transition through the abrupt emergence of some  $5f$ -electronic states at 45 K in  $USb_2$  [8]. In contrast, Feng *et al.* only observed continuous evolution of the tunneling spectra with temperature, indicating the crossover behavior for the localized-itinerant transition of  $5f$  electrons [9]. Meanwhile, except for  $USb_2$ , STM/STS studies of other  $UX_2$  compounds are still lacking. Performing more STM/STS studies on  $UX_2$  can help us to clarify these controversial issues, including the complex relations between AFM and Kondo entanglement and also the discrepancy in the reported STM studies.  $UAs_2$ , with the highest  $T_N$  in the  $UX_2$  family [17], is no doubt a good choice for further STM study.

The influence of point defects on the properties of HFs is another important issue in the research of strong-correlation physics. In the reported studies, the magnetic atom vacancy, namely, the Kondo hole, has been extensively studied since it can create a quantum state to effectively suppress the Kondo hybridization and cause an oscillation of electronic structure [18–20]. To explore the Kondo hole related physics, the most widely adopted method is to probe the variations of physical properties under the influence of random Kondo-hole doping

\*liuqin493@163.com

<sup>†</sup>sytan4444@163.com

<sup>‡</sup>lxcydbj@163.com

via macroscopic experimental technique, such as transport measurement [21–27]. By contrast, recent STM/STS studies unambiguously visualized the perturbation and oscillation of electronic structures induced by the individual Kondo holes in  $\text{URu}_2\text{Si}_2$  and  $\text{SmB}_6$  on the atomic scale [20,28]. Although great progress has been made in the research of magnetic atom vacancy, whether nonmagnetic atom vacancy can affect the low-energy excitations in HF compounds remains elusive and there is no corresponding experimental study until now. In the meantime, the previous STM study of  $\text{USb}_2$  has identified Sb-atom vacancies on the Sb-terminated surface [9], implying the general existence of nonmagnetic atom vacancies on the cleaved single crystals of the  $\text{UX}_2$  family. Therefore, performing STM studies on more of the other  $\text{UX}_2$  compounds may provide an opportunity to explore the influences of individual nonmagnetic atom vacancies on the low-energy excitations in HFs.

In the present study, we report the STM/STS study on the As2-terminated surfaces of  $5f$ -electron based antiferromagnet  $\text{UAs}_2$ . The typical  $dI/dV$  spectra reveal five remarkable peaks at low temperatures and they are ascribed to the Crystal-electric-field (CEF) states, KR, and AFM states. The intensity of the KR peak is logarithmically enhanced with decreasing temperature and the analysis of the peak width yields a Kondo coherence temperature of  $69 \pm 2$  K. Surprisingly, the CEF, KR, and AFM states are all locally altered due to the presence of As-atom vacancies, and the KR peak can be strongly suppressed by increasing the number of missing As atoms. Our work demonstrates that the Kondo coherence can be well established deeply inside the AFM phase and coexist with the AFM order in  $\text{UAs}_2$  and it also emphasizes the intricate and indispensable role of nonmagnetic atoms in the formation of various low-energy excitations in a HF compound.

## II. METHODS

High-quality single crystals of  $\text{UAs}_2$  have been synthesized by vapor transport method with  $3\text{--}5$  mg/cm<sup>3</sup> of iodine carrier. Details of the growth procedures can be found in our earlier work [15]. Crystalline quality was confirmed by resistivity transport measurements. The residual resistivity ratios ( $\rho_{300\text{K}}/\rho_{2\text{K}}$ ) all exceed 200, indicating high sample quality and low density of defects (see Fig. S1 in the Supplemental Material [29]). All the STM/STS measurements were carried out by a low-temperature STM apparatus with a base pressure greater than  $5 \times 10^{-11}$  mbar. The high-quality single crystals of  $\text{UAs}_2$  were cleaved perpendicular to the crystallographic  $c$  axis *in situ* in the STM analysis chamber. Clean tungsten tips were used after Ar<sup>+</sup> sputtering and followed by being treated on a clean Cu(111) surface before performing the measurements on  $\text{UAs}_2$ . The tunneling differential conductance ( $dI/dV$ ) spectra were collected by a standard lock-in technique with a modulation amplitude of 2 mV.

## III. EXPERIMENTAL RESULTS

### A. Cleavage surface

$\text{UAs}_2$  crystallizes in the tetragonal anti- $\text{Cu}_2\text{Sb}$  structure with lattice parameters  $a = 3.963$  Å and  $c = 8.097$  Å as shown in the inset of Fig. 1(a). Several high-quality single

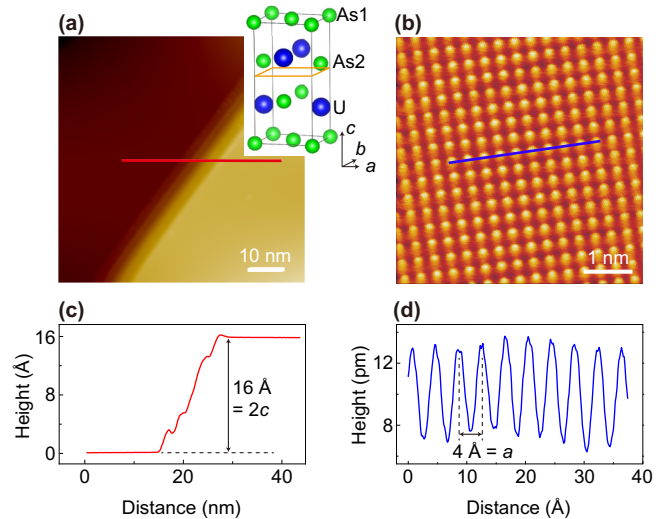


FIG. 1. Topographic STM images and the height profiles of the cleaved surface of  $\text{UAs}_2$ . (a) Typical STM constant-current image of the cleaved surface at 4.5 K ( $V_b = 1.5$  V,  $I = 50$  pA), which exhibits a clean and intact region in the  $a$ - $b$  plane of the tetragonal crystal structure shown in the inset. Inset: Schematic view of the lattice structure of  $\text{UAs}_2$ . (b) Atomically resolved STM image of the (001) surface of  $\text{UAs}_2$  ( $V_b = 0.1$  V,  $I = 100$  nA). (c) Height profile measured across the red line through the surface in panel (a). The height between two step terraces is twice the lattice parameter  $c$ . (d) Height profile measured across the blue line in panel (b). The distance between two neighboring atoms is 4 Å.

crystals of  $\text{UAs}_2$  are cleaved perpendicular to the  $c$  axis *in situ* in the STM analysis chamber with a base pressure greater than  $5 \times 10^{-11}$  mbar. Figure 1(a) shows a typical large-scale topographic image taken on the cleaved surface of  $\text{UAs}_2$ . Clean and flat terraces were observed in a large number of imaged areas and the step height between two neighboring terraces is usually the integer multiple of the lattice constant,  $c$  of bulk  $\text{UAs}_2$ . For instance, the measured height profile across two flat terraces in Fig. 1(a) yields a step height of 16 Å, which is just twice the value of  $c$  [Fig. 1(c)]. A step height equal to the an integer multiple of  $c$  also implies that the upper and the lower terrace in Fig. 1(a) should have the same surface atomic structures. Atomically resolved topographic images reveal a tetragonal lattice structure, with an atomic spacing of 4 Å [Fig. 1(d)]. This implies that the cleavage surface in Fig. 1 corresponds to either a U- or As2-terminated surface, since both of them exhibit the same tetragonal lattice structure. However, previous studies have reported that the cleavage plane of  $\text{UX}_2$  ( $X=\text{Sb}, \text{As}$ ) compounds is expected to take place between the neighboring  $X_2$  surfaces [7–9]. As shown in Fig. S2 (in the Supplemental Material [29]), cleavages occurring at any other planes, i.e., As1-U or As2-U, will result in two different terminated surfaces. In fact, only when the cleavage takes place at the As2-As2 plane [marked by orange squares in the inset of Fig. 1(a)], it can produce two equivalent terminations. Based on the images recorded on plenty of areas after the cleavages of three different samples, only one kind of lattice structure, i.e., the tetragonal lattice shown in Fig. 1(b), has been observed and all the  $dI/dV$  curves taken on the clean regions of cleaved surfaces exhibit the same

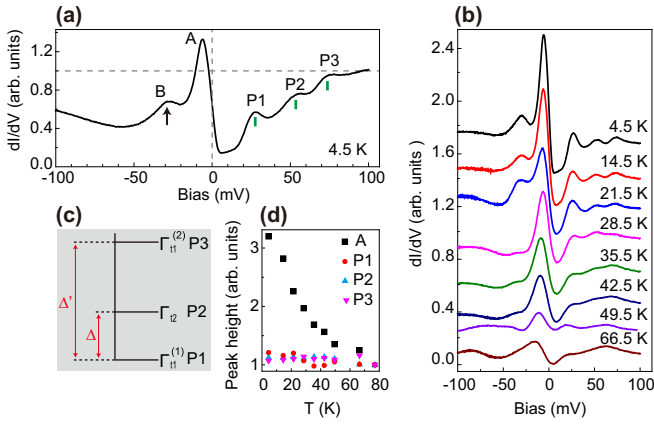


FIG. 2. Typical  $dI/dV$  spectra on the As2 termination of  $UAs_2$  and its temperature evolution. (a) Typical  $dI/dV$  spectrum taken in the clean region of the As2-terminated surface at 4.5 K. The spectrum is normalized to the data at +100 mV. (b) Temperature evolution of the  $dI/dV$  spectra of  $UAs_2$ . All the spectra were taken in the same clean region of the As2-terminated surface. To eliminate the effect of thermal broadening, they were subtracted by the data taken at 77 K and shifted vertically for clarity. All the measured raw data are shown in Fig. S3 [29]. The schematic of the crystal-field splitting states with the splitting energy  $\Delta$  and  $\Delta'$  of the  $U^{4+}$  ion in bulk  $UAs_2$  [17]. (d) Temperature evolutions of the peak heights extracted from panel (b). The heights of peak A and CEF peaks (denoted as P1–P3 in panel (a)) are represented by different color marks, respectively.

spectral feature around  $E_F$ . These observations hence confirm that the cleaved surfaces are the As2-terminated surface and all the following STM/STS measurements were carried out on the As2 terminations.

### B. Overview of STS and CEF states

Figure 2(a) shows the typical  $dI/dV$  spectrum measured on the As2-terminated pristine surface at 4.5 K. Five peaks are distinctly observed in the tunneling spectrum. Among them, three peaks (labeled P1–P3) always reside above  $E_F$  and respectively locate at around +28, +53, and +78 mV. Below  $E_F$ , there are two peaks located at around –30 mV (denoted as peak B) and –6 mV (denoted as peak A), respectively. To explore the origins of these spectral features, we performed variable temperature measurements from 4.5 to 77 K [Fig. 2(b)]. Remarkably, peak A exhibits an obvious temperature-dependent behavior, whereas peak B can be clearly observed at lower temperatures and it seems to merge with peak A to form a broader peak above 49.5 K due to thermal broadening [Fig. 2(b)]. The origins of peaks A and B will be discussed in detail later.

According to molecular field approximation, Amoretti *et al.* predicted a three-level energy scheme caused by the crystal-field splitting of the  $U^{4+}$  ion in  $UAs_2$  as shown in Fig. 2(c) [17]. Since peaks A and B are ascribed to other origins and exhibit different behaviors as a function of temperature and atom vacancy as discussed later, the three peaks, P1–P3 above  $E_F$ , are proper candidates for the theoretically predicted crystal-field splitting states based on the following reasons. Firstly, the heights of peaks P1–P3 vary very slowly

with temperature compared to that of peak A [Fig. 2(d)] and their energy positions remain almost unchanged with increasing temperature (Fig. S4 [29]). These temperature evolutions comply well with the reported behaviors of the CEF states in other  $4f$ -electron based HF systems [29,30]. Secondly, the CEF excitation states of  $U^{4+}$  in  $UAs_2$ , i.e., an electron system with unoccupied CEF levels, are expected to locate within positive bias voltages in the  $dI/dV$  spectrum, which agrees well with our experimental observations, and this is consistent with the previously reported cerium-based ( $4f^1$ ) electron system and just the opposite of the ytterbium-based ( $4f^{14}$ ) hole system [4,30]. Besides, the calculated splitting energies  $\Delta$  and  $\Delta'$  between the three singlets  $\Gamma_{11}^{(2)}$ ,  $\Gamma_{12}$ , and  $\Gamma_{11}^{(1)}$  are on the same order of magnitude as the energy separations between the three peaks P1–P3 in the  $dI/dV$  spectrum [17]. We note that P1–P3 show different behaviors with the emergence of As-atom vacancies as detailed later (in Sec. III D). P2 and P3 merge together, while the energy positions of peaks B and P1 remain nearly unchanged on single-atom vacancy. This phenomenon seems to imply that P1 may also originate from AFM. But for this scenario, the dilemma is that one crystal-field state is missing, since the theoretical work predicts that there are three CEF states in  $UAs_2$  [17]. Even though, we cannot fully exclude this possibility and neutron scattering experiments can help to further clarify this issue in the future.

### C. Kondo resonance and AFM state

We now explore the origins of peaks A and B. Peak A locates slightly below  $E_F$  and it exhibits an asymmetric line shape as well as a strongly temperature-dependent behavior [Figs. 2(a) and 2(d)]. These features highly resemble the characters of the well-studied Kondo resonance state in those famous  $4f$ - or  $5f$ -electron based HF systems [9,29,31,32]. Moreover, our previous temperature-dependent Angle-resolved photoemission spectroscopy (ARPES) measurement of  $UAs_2$  has found two nearly flat bands  $\alpha$  and  $\beta$  and confirmed that they respectively arise from the Kondo hybridization and the AFM phase transition [33], and their energy positions (–6 and –29.8 meV) are almost equal to the energy levels of peaks A and B, respectively. This phenomenon supports our ascription of peak A to Kondo resonance and it also provides an important clue to the origin of peak B, i.e., the AFM state. In scanning tunneling spectroscopies, Kondo resonance is manifested as an asymmetric line shape, which is aroused by the quantum interference between the tunneling from the tip to the  $f$ -electron dominated resonance state and to the itinerant electron states [5,6,34], and the spectral structure can be described by the two-channel Fano formula [5,6,35]:

$$dI/dV(\varepsilon) \propto \left( \frac{\varepsilon - \varepsilon_0}{\Gamma} + q \right)^2 / \left[ 1 + \left( \frac{\varepsilon - \varepsilon_0}{\Gamma} \right)^2 \right], \quad (1)$$

where  $\varepsilon_0$  represents the energy position of Fano resonance relative to  $E_F$ ,  $q$  is the asymmetric parameter of the line shape, and  $\Gamma$  is the half width at half maximum (HWHM) of the resonance curve. Meanwhile, an AFM state can be described by a Lorentz line shape [35,36]. Therefore, to simultaneously extract various pieces of information of peaks A and B, a Fano + Lorentz fit with a small linear background is applied to

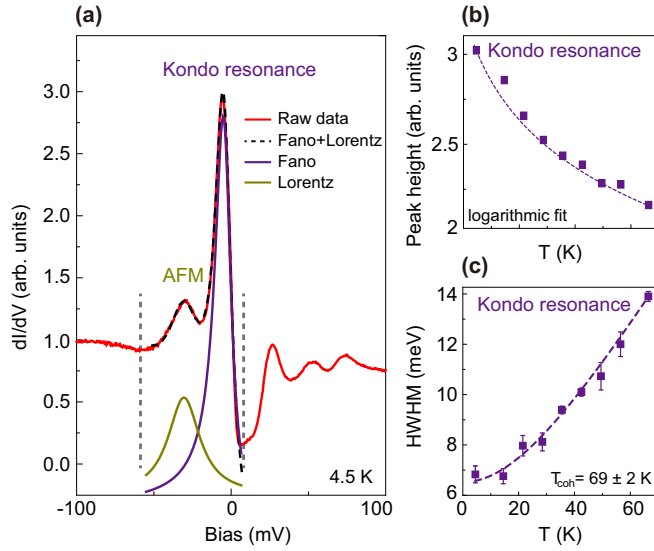


FIG. 3. Analysis of Kondo lattice and AFM peaks of  $\text{UAs}_2$ . (a) Fitting of the typical  $dI/dV$  spectrum of  $\text{UA}_2$ . The spectrum is normalized to the data at +100 mV. The black dashed line is an optimized Fano + Lorentz fit with a linear background term, which is expressed as  $g(\varepsilon) = a\text{Fano}(\varepsilon) + \text{Lorentz}(\varepsilon) + b\varepsilon + c$ . The purple and dark yellow lines respectively represent the plotted individual Fano and Lorentz curves based on the parameters obtained by the fitting. The height as well as the HWHM of the Fano resonance at various temperatures can be extracted from the fittings and represented as squares in panels (b,b), respectively. (b) The KR peak height as a function of temperature. The peak heights are read from the Fano fitting curves. The dashed line is a logarithmic fit. (c) The extracted HWHM of Fano resonance as a function of temperature. The dashed line is the temperature dependence of the HWHM fitted by Eq. (2).

the  $dI/dV$  spectrum within negative biases [Fig. 3(a)]. More details about the choice of the fitting method are shown in Sec. S4 of the Supplemental Material [29].

Figure 3(b) shows the height of peak A as a function of temperature. The increase of the peak height with temperature follows a logarithmic rule, which is a universal behavior in HF materials aroused by the coherent Kondo scattering [37]. For the single-impurity Kondo model, finite temperatures induce thermal broadening of the HWHM of the KR state and the temperature evolution of HWHM in the Fermi liquid regime can be described by the following relation [38]:

$$\text{HWHM} = \sqrt{(\pi k_B T)^2 + 2(k_B T_K)^2}, \quad (2)$$

where  $k_B$  is Boltzmann's constant and  $T_K$  is the Kondo temperature. STM/STS studies in  $5f$  or  $4f$ -electron based HF compounds, e.g.,  $\text{USb}_2$  [7–9,14],  $\text{UGe}_2$  [39],  $\text{URu}_2\text{Si}_2$  [40], and  $\text{YbRh}_2\text{Si}_2$  [5,29], find that the coherent Kondo state residing in the  $f$  levels of a periodic lattice also exhibits the exponential temperature dependence. Through analogy to Eq. (2), the HWHM of the coherent Kondo state can be phenomenologically expressed by  $\Gamma = \sqrt{(\pi k_B T)^2 + 2(k_B T_{\text{coh}})^2}$ , where  $T_{\text{coh}}$  corresponds to the Kondo coherence temperature. As shown by the fitting curve (dashed line) in Fig. 3(c), this model successfully describes the temperature evolution of

peak A in  $\text{UAs}_2$  and the fit yields  $T_{\text{coh}} = 69 \pm 2$  K. Meanwhile, a broad peak emerges at around 70 K in the  $c$  axis thermoelectric power  $S(T)$  curve of  $\text{UAs}_2$  single crystal [41], which was also ascribed to Kondo coherence. Obviously, the  $T_{\text{coh}}$  of  $\text{UAs}_2$  determined by our STS measurements is quite consistent with the onset temperature of the broad peak in transport measurement.

According to the fitting results (Fig. S6 [29]), the energy position of peak B fluctuates around  $-30$  mV and it does not show any obvious trends in the measured temperature range [4.5, 66.5 K], which is far below  $T_N$ . In contrast, the energy position of the KR peak shifts towards lower energies with increasing temperatures. These observations are in good agreement with the temperature evolutions of the electronic structures induced by the Kondo hybridization and AFM transition reported before [7,15]. In the ARPES study, the AFM gap opens at 273 K; thus the energy position of its leading edge, which corresponds to band  $\beta$ , almost remains unchanged below 80 K. This agrees with the behavior of peak B as shown in Fig. S6 [29]. In addition, peak B shows similar characteristics with other reported magnetic compounds as follows: (1) Clearly separated from the KR band (peak) in momentum (energy) position; (2) rather weak temperature-dependent behavior far below the magnetic phase transition temperature [7–10,35,36]. Based on the above points, the most possible origin of peak B is AFM.

The AFM and KR states are simultaneously observed in the tunneling spectra of  $\text{UAs}_2$ , violating the conventional expectation that the two will compete with each other. The Kondo coherence develops deeply in the well-established antiferromagnetic ordered state and it exhibits a sharp resonance peak, which is undisturbed by the antiferromagnetic order as proved by the logarithmic increase of intensity with temperature. This phenomenon corroborates the existence of the itinerant  $5f$  electrons in the antiferromagnetic ordered state of  $\text{UAs}_2$ . In addition, the temperature evolutions of all the five peaks are continuous, and we did not observe any distinctly “abrupt change” [8] in the measured temperature range.

#### D. Influence of As-atom vacancies on CEF, AFM, and KR states

In the atomically resolved STM image, some surface defects can be observed on the As2-terminated surfaces (Fig. S7(a) [29]). One kind of defect appears as dimmed holes under different imaging voltages, always located at the surface As2 sites (see Figs. S7(b)–S7(h) and Sec. S6 [29]). Therefore the dimmed holes are rationally assigned to surface As-atom vacancies. In Fig. 4(a), we compare the typical tunneling spectra of a single-As-atom vacancy, double-As-atom vacancy and intact region on the As2 termination at 4.5 K. For the CEF states, the most striking alteration is that the P2 and P3 states seemingly merge into a single peak around both single- and double-atom vacancies. Since crystal-field splitting is related to the local symmetry, coordination, and electric charge of U and As atoms in the crystal structure, the emergence of As-atom vacancies locally alters these properties and consequently alters the crystal-field splitting. Our precise determination of these CEF states in the STSs can put strong constraints on the related future theoretical calculations.

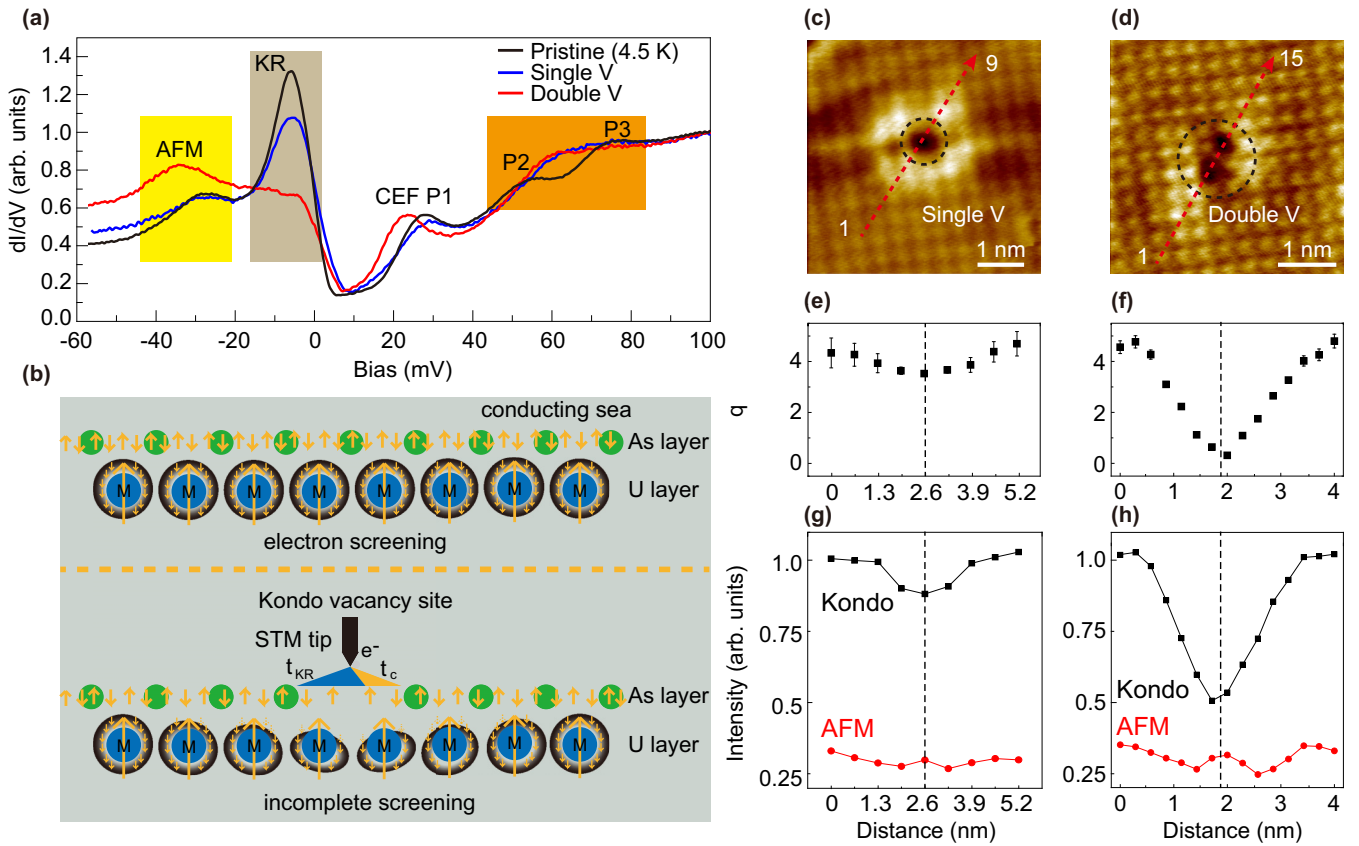


FIG. 4. Spatially tuning the Kondo resonance and AFM states through the As-atom vacancies. (a) The  $dI/dV$  spectra measured on the single-atom vacancy, double-atom vacancy, and intact region on the As<sub>2</sub>-terminated surface at 4.5 K. (b) The schematic view of the Kondo screening in UAs<sub>2</sub> (upper panel) and the incomplete Kondo screening caused by surface As-atom vacancy (lower panel). The blue circles represent the localized U magnetic moments surrounded by the spin-flipped conduction electrons represented by small orange arrows. This schematic mainly reflects the two interfering tunneling paths and the incomplete Kondo screening induced by As-atom vacancy. (c), (d) Atomically resolved STM images of the (c) single-atom vacancy ( $V_b = 0.2$  V,  $I = 150$  nA) and (d) double-atom vacancy ( $V_b = 0.2$  V,  $I = 200$  nA). A series of  $dI/dV$  spectra were measured along the red dashed lines and the measured  $dI/dV$  spectra and their corresponding detecting positions are shown in Figs. 5(a) and 5(g). (e), (f) The spatial dependence of the Fano asymmetry parameter  $q$  across the (e) single-atom vacancy and (f) double-atom vacancy. The values of  $q$  are extracted from the Fano + Lorentz fits to the series of  $dI/dV$  spectra shown in Fig. 5. (g), (h) The spatial dependence of the intensities (or heights) of the Kondo resonance and AFM peaks extracted from the Fano + Lorentz fits across (g) single-atom vacancy and (h) double-atom vacancy. The vertical dashed line in panels (e), (h) marks the center of the single-atom vacancy or double-atom vacancy.

The KR peak exhibits a reduction in intensity on both As-atom vacancies. In contrast to the Fe(II)-atom vacancy in Fe<sub>3</sub>GeTe<sub>2</sub> [36], which acts as “Kondo hole” and counterintuitively strengthens the KR state, the As-atom vacancy in UAs<sub>2</sub> behaves as a nonmagnetic counterpart of the Kondo hole and induces an opposite alteration of the KR state. In spite of the bulk antiferromagnetism in UAs<sub>2</sub>, there is ferromagnetic correlation between the in-plane magnetic atoms in the U-atomic layer underneath the outmost As<sub>2</sub> layer, analogous to the case of the two-dimensional ferromagnetic Fe<sub>3</sub>GeTe<sub>2</sub> [36]. The Kondo screening effect on the intact surface together with a locally incomplete screening model of the magnetic moments are shown in Fig. 4(b). The number of the itinerant conduction electrons is reduced due to the absence of As atoms, which locally weakens the effective screening of the magnetic moment. Hence, the Kondo resonance is locally suppressed and leads to a reduction of peak intensity. The statistics of the KR peak heights on top of various single-atom vacancies, double-atom vacancies, and intact regions are

shown in Fig. S8 [29]. For double-atom vacancies, the average intensity of KR peaks decreases to around 53% of that on the intact sites, whereas for single-atom vacancies, it decreases to around 87%. These results confirm that the suppression of the Kondo resonance drastically augments as the number of missing conduction atoms increases.

To investigate the spatial modulation effect caused by the vacancies, a series of  $dI/dV$  spectra were taken across the single-atom vacancy and the double-atom vacancy as shown in Fig. 5. The  $q$  values and the intensities of KR and AFM states extracted from Fano + Lorentz fits are displayed as a function of distance in Figs. 4(e)–4(h). For the single-atom vacancy,  $q$  drops by  $\sim 20\%$  (from 4.25 to 3.28) as the tip is moved from the intact region to the vacancy center and the KR intensity exhibits a similar decreasing trend when approaching the center. For the double-atom vacancy, both  $q$  and KR intensity display a much stronger decreasing trend with distance, and  $q$  drops by  $\sim 90\%$  (from 4.2 to 0.32) at the vacancy center. For the Fano resonance, the  $q$  value is determined

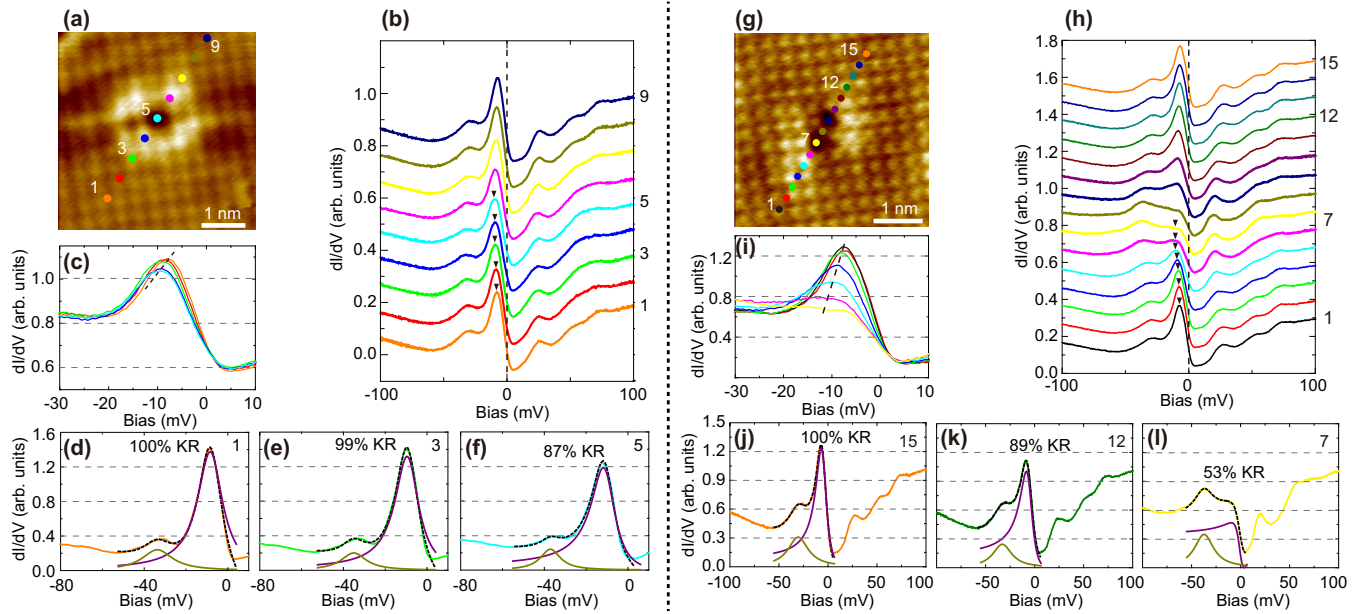


FIG. 5. A series of  $dI/dV$  spectra measured across the single-atom vacancy (left panel) and double-atom vacancy (right panel) with their Fano + Lorentz fits. (a), (g) Atomically resolved STM images ( $V_b = 5$  mV,  $I = 400$  pA) of the single-atom vacancy (a) and double-atom vacancy (g). The colored dots mark the positions where those spectra in panels (b), (h) were taken, respectively. (b), (h) A series of  $dI/dV$  spectra measured along the colored dots labeled by 1–9 in panel (a) or labeled by 1–15 in panel (g). These spectra are normalized to the data at +100 mV and then offset for clarify. The energy positions of the KR state are marked by black arrows. (c), (i) Direct comparison of the normalized  $dI/dV$  spectra detected at positions 1–5 around single-atom vacancy (c) and 1–7 around double-atom vacancy (i). The energy positions of the KR states at different sites are marked by the dashed lines. (d)–(f) The Fano + Lorentz fitting details of the spectra detected at positions 1, 3, and 5 with their relative KR intensity labeled around single-atom vacancy. (j)–(l) The Fano + Lorentz fitting details of the spectra detected at positions 15, 12, and 7 with their relative KR intensity labeled. The black dashed lines are the optimized Fano + Lorentz fitting curves. The purple and dark yellow lines respectively represent the plotted individual Fano and Lorentz curves based on the parameters obtained by the multi-peaks fitting.

by the relative strength between the indirect tunneling into the many-body KR state ( $t_{KR}$ ) and direct tunneling into the itinerant conduction electrons ( $t_c$ ) [42]. A  $q$  value much larger than 1 (i.e.,  $q \sim 4$ ) on the intact regions implies that electrons mainly tunnel into the Kondo-screened  $U-5f$  states rather than the itinerant electronic states; even the outmost atomic layer merely consists of As rather than U atoms. It is noteworthy that STM/STS studies on  $URu_2Si_2$  [40] or  $CeCoIn_5$  [18] find that the strength of tunneling into the heavy  $5f$  or  $4f$  states is more pronounced on the Si or Co layer instead of the U or Ce-In layer. And the tunneling process in  $USb_2$  is also dominated by the tunneling channel into the screened  $U-5f$  states on the Sb termination [8,9]. These similar phenomena indicate that the orientation of atomic orbitals and the selective hybridization among different suborbitals are crucial for the quantum interference tunneling in the Kondo lattice, and the stronger coupling to the heavy  $5f$  states on the  $As_2$  layers in  $UAs_2$  is probably caused by the larger amplitude of hybridization of  $f$  electrons with the out of plane  $sp$  electrons than that with the in-plane  $sp$  electrons, analogous to the theoretical model established in  $CeIrIn_5$  [43]. To the contrary, on those As-atom vacancies, the underneath U atoms are exposed and hence the direct tunneling into the itinerant conduction electrons is enhanced and the indirect tunneling into the  $5f$  electron dominated KR state is correspondingly suppressed, leading to the decrease of  $q$ . The more surface As atoms

miss, the more U atoms are exposed, which further reduces  $q$  value on the double-atom vacancy as compared with single-atom vacancy. Such a small  $q$  value ( $<1$ ) suggests that the quantum interference tunneling is already dominated by the direct tunneling channel into itinerant conduction electrons on double-atom vacancies.

Compared to the apparent suppression of the KR state, the influence of As-atom vacancies on the AFM state is much weaker [red dots in Figs. 4(g) and 4(h)]. When approaching the center of either vacancy from intact regions, the intensity of the AFM peak at first decreases to reach a local minimum and then increases to reach a local maximum at the center. Again, the spatial alterations of the AFM peak induced by double-atom vacancy are relatively stronger and wider than those induced by single-atom vacancy. Even the local maximum emerges at the vacancy center; its intensity is just similar with those detected away from the center. More theoretical calculations and simulations are required to elucidate the complex spatially dependent fluctuation of the AFM state and its relation with the KR state around As-atom vacancies in the future.

#### IV. DISCUSSION

Our STM studies have provided several important insights into the interpretation of the HF physics. One is about how

the Kondo interaction evolves with temperature. In  $\text{UAs}_2$ , the hybridization between the localized  $5f$  electrons and itinerant conduction electrons, i.e.,  $f$ - $c$  hybridization, starts to appear above 290 K as revealed by the ARPES study [15], whereas our STM/STS studies suggest the full formation of Kondo coherence occurs at 69 K, which is well below the starting temperature of the  $f$ - $c$  hybridization [29,35]. In fact, we believe that the considerable discrepancy between the two onset temperatures determined by ARPES and STS emphasizes the two-stage process for the heavy electron development in the Kondo lattice [13,44–46]. This difference coincides with the recently proposed Kondo coherence theory [47], in which the short-range Kondo hybridization starts at higher temperatures and the formation of long-range Kondo coherence between Kondo singlets occurs at lower temperatures.

The second issue is about the complex interplay between Kondo hybridization and RKKY interaction in HF systems. Our work corroborates that  $f$ - $c$  hybridization can coexist with the antiferromagnetic order in  $\text{UAs}_2$  and Kondo coherence develops robustly in the antiferromagnetic background. Note that the AFM related peak feature is directly detected on the As2 termination of  $\text{UAs}_2$ , whereas it is absent on the Sb termination of  $\text{USb}_2$  [9]. The emergence of the AFM state on the As2 termination should be ascribed to the much higher  $T_N$  and smaller interatomic (U-X) distances in  $\text{UAs}_2$  as compared with  $\text{USb}_2$ . But the question about exactly how the Kondo hybridization and magnetic ordered state coexist with each other in  $\text{UAs}_2$  is still unclear. The orbital-selectivity scenario proposed in  $\text{CeSb}$  or  $\text{USb}_2$  is the most probable reason [7,10]. Yet, the exact manner of orbital selection can vary considerably in different systems. For instance, in  $\text{CeSb}$ , it is determined by the conduction electron states; i.e., different conduction bands respectively participate in the formation of Kondo hybridization and the AFM state [10], whereas in  $\text{USb}_2$ , different  $5f$  suborbitals selectively participate in the two interactions [7]. For  $\text{UAs}_2$ , it is confirmed that the flat  $\alpha$  and  $\beta$  bands, which are separated in the momentum space, are respectively related with the Kondo hybridization and AFM order [15]. Yet, photoemission measurements with different polarized photons have not detected obvious differences between these two bands, like those observed in  $\text{USb}_2$ . Further orbital-resolved investigations, like DMFT calculations, are necessary in the future to help to identify the orbital characters and clearly unveil the mechanism of the coexistence of AFM and KR states in  $\text{UAs}_2$ .

The last issue involves the microscopic electronic phenomenology of the atom vacancy in the HF lattice. The study of As-atom vacancies deepens our cognition of Kondo physics. A considerable number of experimental and theoretical studies have focused on the impacts of Kondo holes, i.e., surface defects substituting or removing a  $f$ -contributing moment, on the electronic structures of HFs [19,20,48]. By contrast, the influence of the nonmagnetic-atom vacancy on the electronic states has not attracted much attention in Kondo lattice. One may intuitively suspect that the influence of nonmagnetic atom vacancies should be weak or even absent as compared with that of magnetic atom vacancies, because the  $f$  electrons in magnetic atoms are the basis of heavy fermion systems. However, our STM observations demonstrate that nonmagnetic atom vacancies can impose an observable or

even drastic alteration on the Kondo resonance state (as well as the AFM and CEF states) depending on the number of missing atoms. Additionally, when the tip is moved from the intact region to the As-atom vacancy center, the energy position of the KR state gradually shifts towards the direction away from the Fermi level [see Figs. 5(b) and 5(c), and 5(h) and 5(i)], indicating the shift of the renormalized  $f$  band. In fact, the emergence of either magnetic or nonmagnetic atom vacancies alters the quantity of charge carriers in a uniform Kondo lattice. As a consequence, the hybridized Fermi surface reshapes to maintain the uniform  $f$ -electron density, resulting in the corresponding shifting of KR energy [49]. In short, the conduction-electron density in a Kondo lattice plays a decisive role in determining the KR energy. Recently, similar shifting of the KR energy level towards the opposite direction has been observed around the Kondo holes in  $\text{URu}_2\text{Si}_2$  and  $\text{SmB}_6$  [49]; this behaves as the counterpart of the missing nonmagnetic atom and shows excellent consistency with our observation. Whether these nonmagnetic atom vacancies in  $\text{UAs}_2$  can lead to long-range hybridization oscillations, like those observed in Th-doped  $\text{URu}_2\text{Si}_2$  or Fe-doped  $\text{SmB}_6$  [20], remains an open question. The newly developed gap map of “rectification” [49] may help to verify this issue in the future.

## V. CONCLUSIONS

In summary, the CEF, AFM, and KR related spectral features are simultaneously detected in the STS images taken on the As2 terminations of  $\text{UAs}_2$ . The logarithmical enhancement behavior of the KR peak with decreasing temperature demonstrates the coexistence of Kondo coherence with AFM order and confirms the dual characters of itinerancy and localization for the  $5f$  electrons in  $\text{UAs}_2$ . The divergence between the  $T^*$  determined by ARPES and the  $T_{\text{coh}}$  determined by STS reveals the difference between the onset of  $f$ - $c$  hybridization and the full establishment of long-range Kondo coherence. Surprisingly, the nonmagnetic atom vacancies in  $\text{UAs}_2$  apparently affect the KR, CEF, and AFM states and induce the energy shifting of the KR peak, which highlights the importance of the easily overlooked nonmagnetic atoms in a Kondo lattice. Our results provide an illuminating insight into various low-energy excitations and their complex interactions in the  $5f$ -electron based antiferromagnetic HF materials, including the intricate interplay between AFM order and the Kondo effect, the difference between the onset of  $f$ - $c$  hybridization and the formation of Kondo coherence, and the indispensable role of the nonmagnetic atoms in a Kondo lattice.

All data needed to evaluate the conclusions in the paper are present in the paper and/or the Supplemental Material [29]. Additional data related to this paper may be requested from the authors.

## ACKNOWLEDGMENTS

We gratefully acknowledge helpful discussions with Prof. Y. F. Yang, D. L. Feng, and J. Jiang. This work is supported by the National Key Research and Development Program of China (Grants No. 2021YFA1601101 and No. 2022YFA1402201) and the National Natural Science

Foundation of China (Grants No. U23A20580, No. 12004349, No. 11904335, No. 12122409, No.11974319, No. 21903074, No. 11904334, and No. 11774320).

X.Y.J., Q.L., S.Y.T., and X.C.L. conceived the experiment. X.Y.J. and Y.L. synthesized single crystals and performed

the transport measurement. Y.Z., W.F., Q.Q.H., X.G.Z., Q.Z., Q.Y.C. and X.B.L. discussed the experimental results and provide valuable suggestions. Q.L. and X.Y.J. performed the STM measurements.

The authors declare no competing financial interests.

- 
- [1] G. R. Stewart, Heavy-fermion systems, *Rev. Mod. Phys.* **56**, 755 (1984).
- [2] Z. Fisk, J. L. Sarrao, J. L. Smith, and J. D. Thompson, The physics and chemistry of heavy fermions, *Proc. Natl. Acad. Sci. USA* **92**, 6663 (1995).
- [3] M. A. Ruderman and C. Kittel, Indirect exchange coupling of nuclear magnetic moments by conduction electrons, *Phys. Rev.* **96**, 99 (1954).
- [4] J. Kondo, Resistance minimum in dilute magnetic alloys, *Prog. Theor. Phys.* **32**, 37 (1964).
- [5] S. Seiro, L. Jiao, S. Kirchner, S. Hartmann, S. Friedemann, C. Krellner, C. Geibel, Q. Si, F. Steglich, and S. Wirth, Evolution of the Kondo lattice and non-Fermi liquid excitations in a heavy-fermion metal, *Nat. Commun.* **9**, 3324 (2018).
- [6] S. Paschen, S. Friedemann, S. Wirth, F. Steglich, S. Kirchner, and Q. Si, Kondo destruction in heavy fermion quantum criticality and the photoemission spectrum of YbRh<sub>2</sub>Si<sub>2</sub>, *J. Magn. Magn. Mater.* **400**, 17 (2016).
- [7] Q. Y. Chen, X. B. Luo, D. H. Xie, M. L. Li, X. Y. Ji, R. Zhou, Y. B. Huang, W. Zhang, W. Feng, and Y. Zhang, Orbital-selective Kondo entanglement and antiferromagnetic order in USb<sub>2</sub>, *Phys. Rev. Lett.* **123**, 106402 (2019).
- [8] I. Giannakis, J. Leshen, M. Kawai, S. Ran, C. J. Kang, S. R. Saha, Y. Zhao, Z. Xu, J. W. Lynn, L. Miao, L. A. Wray, G. Kotliar, N. P. Butch, and P. Aynajian, Orbital-selective Kondo lattice and enigmatic *f* electrons emerging from inside the antiferromagnetic phase of a heavy fermion, *Sci. Adv.* **5**, eaaw9061 (2019).
- [9] W. Feng, D. H. Xie, X. B. Luo, S. Y. Tan, Y. Liu, Q. Liu, Q. Q. Hao, X. G. Zhu, Q. Zhang, Y. Zhang, Q. Y. Chen, and X. C. Lai, Crossover behavior of the localized to itinerant transition of *5f* electrons in the antiferromagnetic Kondo lattice USb<sub>2</sub>, *Phys. Rev. B* **104**, 235103 (2021).
- [10] S. Jang, R. Kealhofer, C. John, S. Doyle, J. S. Hong, J. H. Shim, Q. Si, O. Erten, J. D. Denlinger, and J. G. Analytis, Direct visualization of coexisting channels of interaction in CeSb, *Sci. Adv.* **5**, eaat7158 (2019).
- [11] S. Doniach, The Kondo lattice and weak antiferromagnetism, *Physica B+C (Amsterdam)* **91**, 231 (1977).
- [12] S. Fujimori, Y. Takeda, T. Okane, Y. Saitoh, A. Fujimori, H. Yamagami, Y. Haga, E. Yamamoto, and Y. Onuki, Electronic structures of uranium compounds studied by soft x-ray photoelectron spectroscopy, *J. Phys. Soc. Jpn.* **85**, 062001 (2016).
- [13] Q. Y. Chen, D. F. Xu, X. H. Niu, J. Jiang, R. Peng, H. C. Xu, C. H. P. Wen, Z. F. Ding, K. Huang, L. Shu, Y. J. Zhang, H. Lee, V. N. Strocov, M. Shi, F. Bisti, T. Schmitt, Y. B. Huang, P. Dudin, X. C. Lai, S. Kirchner *et al.*, Direct observation of how the heavy-fermion state develops in CeCoIn<sub>5</sub>, *Phys. Rev. B* **96**, 045107 (2017).
- [14] L. Miao, R. Basak, S. Ran, Y. S. Xu, E. Kotta, H. W. He, J. D. Denlinger, Y. D. Chuang, Y. Zhao, Z. Xu, J. W. Lynn, R. Jeffries, S. R. Saha, I. Giannakis, P. Aynajian, C. J. Kang, Y. L. Wang, G. Kotliar, N. P. Butch, and L. A. Wray, High temperature singlet-based magnetism from Hund's rule correlations, *Nat. Commun.* **10**, 8 (2019).
- [15] X. Ji, X. Luo, Q. Chen, W. Feng, Q. Hao, Q. Liu, Y. Zhang, Y. Liu, X. Wang, S. Tan, X. Lai *et al.*, Direct observation of coexisting Kondo hybridization and antiferromagnetic state in UA<sub>s2</sub>, *Phys. Rev. B* **106**, 125120 (2022).
- [16] H. Siddiquee, C. Broyles, E. Kotta, S. Liu, S. Peng, T. Kong, B. Kang, Q. Zhu, Y. Lee, L. Ke, H. Weng, J. D. Denlinger, L. A. Wray, and S. Ran, Breakdown of the scaling relation of anomalous Hall effect in Kondo lattice ferromagnet USbTe, *Nat. Commun.* **14**, 527 (2023).
- [17] G. Amoretti, A. Blaise, and J. Mulak, Crystal-field interpretation of the magnetic-properties of UP<sub>2</sub>, UAs<sub>2</sub>, USb<sub>2</sub>, UBi<sub>2</sub> compounds, *J. Magn. Magn. Mater.* **42**, 65 (1984).
- [18] P. Aynajian, E. H. da Silva Neto, A. Gyenis, R. E. Baumbach, J. D. Thompson, Z. Fisk, E. D. Bauer, and A. Yazdani, Visualizing heavy fermions emerging in a quantum critical Kondo lattice, *Nature (London)* **486**, 201 (2012).
- [19] J. Figgins and D. K. Morr, Defects in heavy-fermion materials: Unveiling strong correlations in real space, *Phys. Rev. Lett.* **107**, 066401 (2011).
- [20] M. H. Hamidian, A. R. Schmidt, I. A. Firmo, M. P. Allan, P. Bradley, J. D. Garrett, T. J. Williams, G. M. Luke, Y. Dubi, A. V. Balatsky, and J. C. Davis, How Kondo-holes create intense nanoscale heavy-fermion hybridization disorder, *Proc. Natl. Acad. Sci. USA* **108**, 18233 (2011).
- [21] C. L. Lin, A. Wallash, J. E. Crow, T. Mihalisin, and P. Schlottmann, Heavy-fermion behavior and the single-ion Kondo model, *Phys. Rev. Lett.* **58**, 1232 (1987).
- [22] F. Steglich, U. Ahlheim, U. Rauchschwalbe, and H. Spille, Heavy fermions and superconductivity—superconducting spectroscopy of non-magnetic impurities in CeCu<sub>2</sub>Si<sub>2</sub>, *Physica B+C (Amsterdam)* **148**, 6 (1987).
- [23] A. L. Delatorre, P. Visani, Y. Dalichaouch, B. W. Lee, and M. B. Maple, Th-doped URu<sub>2</sub>Si<sub>2</sub>- influence of Kondo holes on coexisting superconductivity and magnetism, *Phys. B (Amsterdam)* **179**, 208 (1992).
- [24] J. M. Lawrence, T. Graf, M. F. Hundley, D. Mandrus, J. D. Thompson, A. Lacerda, M. S. Torikachvili, J. L. Sarrao, and Z. Fisk, Kondo hole behavior in Ce<sub>0.97</sub>La<sub>0.03</sub>Pd<sub>3</sub>, *Phys. Rev. B* **53**, 12559 (1996).
- [25] C. Petrovic, S. L. Bud'ko, V. G. Kogan, and P. C. Canfield, Effects of La substitution on the superconducting state of CeCoIn<sub>5</sub>, *Phys. Rev. B* **66**, 054534 (2002).
- [26] J. Paglione, T. A. Sayles, P. C. Ho, J. R. Jeffries, and M. B. Maple, Incoherent non-Fermi-liquid scattering in a Kondo lattice, *Nat. Phys.* **3**, 703 (2007).



- [27] E. D. Bauer, Y. F. Yang, C. Capan, R. R. Urbano, C. F. Miclea, H. Sakai, F. Ronning, M. J. Graf, A. V. Balatsky, R. Movshovich, A. D. Bianchi, A. P. Reyes, P. L. Kuhns, J. D. Thompson, and Z. Fisk, Electronic inhomogeneity in a Kondo lattice, *Proc. Natl. Acad. Sci. USA* **108**, 6857 (2011).
- [28] L. Jiao, S. Rossler, D. Kasinathan, P. F. S. Rosa, C. Y. Guo, H. Q. Yuan, C. X. Liu, Z. Fisk, F. Steglich, and S. Wirth, Magnetic and defect probes of the  $\text{SmB}_6$  surface state, *Sci. Adv.* **4**, 6 (2018).
- [29] See Supplemental Material at <http://link.aps.org/supplemental/10.1103/PhysRevB.109.075158> for the CEF states detected by STM in  $\text{Yb}_2\text{Rh}_2\text{Si}_2$ .
- [30] A. K. Bhattacharjee and B. Coqblin, Influence of crystalline field on Kondo effect—cerium and ytterbium impurities, *Physica B+C* **86**, 511 (1977).
- [31] S. Shen, C. Wen, P. Kong, J. Gao, J. Si, X. Luo, W. Lu, Y. Sun, G. Chen, and S. Yan, Inducing and tuning Kondo screening in a narrow-electronic-band system, *Nat. Commun.* **13**, 2156 (2022).
- [32] W. K. Park, P. H. Tobash, F. Ronning, E. D. Bauer, J. L. Sarrao, J. D. Thompson, and L. H. Greene, Observation of the hybridization gap and Fano resonance in the Kondo lattice  $\text{URu}_2\text{Si}_2$ , *Phys. Rev. Lett.* **108**, 246403 (2012).
- [33] J. Figgins and D. K. Morr, Differential conductance and quantum interference in Kondo systems, *Phys. Rev. Lett.* **104**, 187202 (2010).
- [34] M. Maltseva, M. Dzero, and P. Coleman, Electron cotunneling into a Kondo lattice, *Phys. Rev. Lett.* **103**, 206402 (2009).
- [35] Y. Zhang, H. Y. Lu, X. G. Zhu, S. Y. Tan, W. Feng, Q. Liu, W. Zhang, Q. Y. Chen, Y. Liu, X. B. Luo, D. H. Xie, L. Z. Luo, Z. J. Zhang, and X. C. Lai, Emergence of Kondo lattice behavior in a van der Waals itinerant ferromagnet,  $\text{Fe}_3\text{GeTe}_2$ , *Sci. Adv.* **4**, eaao6791 (2018).
- [36] M. Zhao, B. Chen, Y. Xi, Y. Zhao, H. Xu, H. Zhang, N. Cheng, H. Feng, J. Zhuang, F. Pan, X. Xu, W. Hao, W. Li, S. Zhao, S. Dou, and Y. Du, Kondo holes in the two-dimensional itinerant ising ferromagnet  $\text{Fe}_3\text{GeTe}_2$ , *Nano Lett.* **21**, 6117 (2021).
- [37] Y. F. Yang and D. Pines, Universal behavior in heavy-electron materials, *Phys. Rev. Lett.* **100**, 096404 (2008).
- [38] K. Nagaoka, T. Jamneala, M. Grobis, and M. F. Crommie, Temperature dependence of a single Kondo impurity, *Phys. Rev. Lett.* **88**, 077205 (2002).
- [39] I. Giannakis, D. Sar, J. Friedman, C.-J. Kang, M. Janoschek, P. Das, E. D. Bauer, G. Kotliar, and P. Aynajian, Coexisting Kondo hybridization and itinerant  $f$ -electron ferromagnetism in  $\text{UGe}_2$ , *Phys. Rev. Res.* **4**, L022030 (2022).
- [40] W. Zhang, W. Feng, X. Luo, S. Tan, D. Xie, Y. Liu, Y. Zhang, Q. Hao, Q. Zhang, X. Zhu, Q. Liu, Q. Chen, and X. Lai, Direct observation of the hybridization gap in both the hidden order and large moment antiferromagnetic phases in  $\text{URu}_2\text{Si}_2$ , *Phys. Rev. B* **106**, 165109 (2022).
- [41] Z. Henkie, A. Wojakowski, R. Wawryk, Z. Kletowski, and T. Cichorek, A Kondo-like thermoelectric power behaviour of  $\text{UAsSe}$  ferromagnet, *Physica B (Amsterdam)* **312**, 307 (2002).
- [42] M. Ternes, A. J. Heinrich, and W. D. Schneider, Spectroscopic manifestations of the Kondo effect on single adatoms, *J. Phys.: Condens. Matter* **21**, 053001 (2009).
- [43] J. H. Shim, K. Haule, and G. Kotliar, Modeling the localized-to-itinerant electronic transition in the heavy fermion system  $\text{CeIrIn}_5$ , *Science* **318**, 1615 (2007).
- [44] Y. F. Yang, Two-fluid model for heavy electron physics, *Rep. Prog. Phys.* **79**, 074501 (2016).
- [45] Y. P. Liu, Y. J. Zhang, J. J. Dong, H. Lee, Z. X. Wei, W. L. Zhang, C. Y. Chen, H. Q. Yuan, Y. F. Yang, and J. Qi, Hybridization dynamics in  $\text{CeCoIn}_5$  revealed by ultrafast optical spectroscopy, *Phys. Rev. Lett.* **124**, 057404 (2020).
- [46] D. Q. Hu, J. J. Dong, and Y. F. Yang, Hybridization fluctuations in the half-filled periodic Anderson model, *Phys. Rev. B* **100**, 195133 (2019).
- [47] J. J. Dong and Y. F. Yang, Development of long-range phase coherence on the Kondo lattice, *Phys. Rev. B* **106**, L161114 (2022).
- [48] R. Solle and P. Schlottmann, A simple theory of the Kondo hole, *J. Appl. Phys.* **69**, 5478 (1991).
- [49] H. Pirie, E. Mascot, C. E. Matt, Y. Liu, P. Chen, M. H. Hamidian, S. Saha, X. Wang, J. Paglione, G. Luke, D. Goldhaber-Gordon, C. F. Hirjibehedin, J. C. S. Davis, D. K. Morr, and J. E. Hoffman, Visualizing the atomic-scale origin of metallic behavior in Kondo insulators, *Science* **379**, 1214 (2023).